


In vivo study of a bioactive nanoparticle-gelatin composite scaffold for bone defect repair in rabbits

Guojin Hou¹ · Fang Zhou ¹ · Yan Guo¹ · Zhongwei Yang¹ · Ailing Li^{1,2} · Chen Wang² · Dong Qiu²

Received: 20 February 2017 / Accepted: 21 September 2017 / Published online: 11 October 2017
© Springer Science+Business Media, LLC 2017

Abstract The purpose is to study the in vivo bioactivity of this scaffold and verify its ability to simulate the characteristics of cancellous bone. Twenty-four adult New Zealand white rabbits were divided into three groups. Bone defects above the femoral condylar of both sides were created. A newly designed bioactive nanoparticle–gelatin composite scaffold was implanted to the experimental side, while the control side was left without implantation. The repair of bone defect was monitored by X-ray examination, gross observation, Micro-CT examination and histological observation of the area of bone defect 4, 8 and 12 weeks after surgery. There was void of new bone tissue in medullary cavity in the bone defect area of the control side. In the experimental side, the composite scaffold displayed excellent biodegradability, bioactivity and cyto-compatibility. With the time laps, new bone tissue grew from the edge to center as revealed by both Micro-CT image and staining biopsy, which complies with the “creeping substitution” process. The mechanical properties of the newly designed bioactive nanoparticle–gelatin composite scaffold and the 3-D structure of new bone tissue are comparable to the surrounding cancellous bones. This newly developed bioactive nanoparticle–gelatin composite scaffold possesses good biocompatibility and in vivo

osteogenic capability for bone defect repair. It may be a promising artificial bone grafts.

1 Introduction

At present, bone defects caused by trauma, tumor, infection and fusion operation are common clinical issue, the repair of them is still challenging [1]. Since Jobi Meekren transplanted a portion of a dog’s skull into a defect in one of the cranial bones of a soldier in 1862 [2], bone transplant technology has been used for more than 150 years. Current natural bone substitutes include autografts, allografts and xenografts. Although autologous bone grafting is considered as the golden standard for bone transplantation, it has the risk of postoperative complications at the donor site and the disadvantage of inadequate supplies, which significantly limits its application. Allograft procedures, on the other hand, may lead to immunological rejection (especially for the grafting of large bone fragments) and also may have ethic concerns [3–5].

Nowadays, bone substitutes have become important materials for treating bone defects and are in high demand. The development of new artificial bone substitution materials has become an important topic both in medical and materials science societies. The general requirements for bone substitution materials are: good biological compatibility, appropriate mechanical properties, micro-porous structure allowing the in-growth of new bone tissue, synchronized absorption rate with the new bone growth rate and easiness of being processed into the required size and shape [6]. Currently, there are many bone graft substitute materials such as inorganic materials [hydroxyapatite (HA),

✉ Fang Zhou
zhou.md@126.com

¹ Department of Orthopaedic Surgery, Peking University Third Hospital, No 49, North Garden Rd, HaiDian District 100191 Beijing, China

² Beijing National Laboratory for Molecular Sciences, State Key Laboratory of Polymer Physics and Chemistry, Institute of Chemistry, Chinese Academy of Sciences, 100190 Beijing, China

bioactive glass, etc.] and biodegradable polymers [poly-(lactic acid) (PLA), poly lactic-co-glycolic acid (PLGA), gelatin, etc.] [7, 8]. However, due to the mechanical or bioactivity defects, there still lacks a “perfect” bone grafting material, which can meet all the above requirements.

Traditionally, researches on bone grafting materials mainly focus on three aspects: three dimensional structure, cell adhesion and biocompatibility. Recent, development of tissue engineering technology has allowed the induction of cell differentiation, proliferation, and implantation on biological materials, composite material have thus attracting more and more attention. Besides the conventional micron-sized particles, nano-sized bioactive particles (nBP) were also used to composite with polymers, with the expectation for better mechanical performances [9, 10]. In our previous work, bioactive particles (BP) with controllable sizes and narrow size distribution were synthesized [11] and used as fillers to form composite scaffolds with gelatin [12]. It was found that these scaffold showed good *in vitro* bioactivity and mechanical properties comparable to cancellous bones; they also showed good cyto-compatibility, where cells could adhere, spread, and proliferate very well [12]. We therefore speculate that it may be a promising artificial bone grafting material, however, its *in vivo* performance needs to be evaluated first.

A critical-sized bone defect (CSD) is defined as a defect which cannot heal spontaneously during the lifetime of the animal [3], which only heals with the aid of proper bone substitutes. CSD is considered as the best model to evaluate bone substitution materials. Skull defect model and the distal femoral defect model are the most commonly used CSD.

In the present study, we established a distal femoral bone defect model and implanted the bioactive nanoparticle—gelatin composite scaffold s into the defect sites to evaluate their *in vivo* performance over a period of 3 months. The purpose is to study the *in vivo* bioactivity of this scaffold and verify its ability to simulate the characteristics of cancellous bone.

2 Materials and methods

2.1 Implant

The bioactive nanoparticle—gelatin composite scaffold used in this experiment is provided by Institute of Chemistry, Chinese Academy of Sciences. The preparation process is briefly described as the following. BPs with mean diameters of 14 nm (BP-14) were dispersed in water at a concentration of 20 wt%. Gelatin solution (20 wt%) (Type A from porcine skin, Sigma-Aldrich) were mixed with BP dispersion under stirring at 40 °C for 8 h. The mixtures were casted into

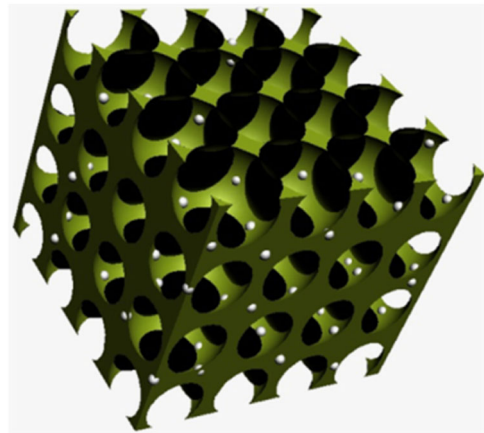


Fig. 1 Three dimensional sketch map of BP-14/gel scaffolds

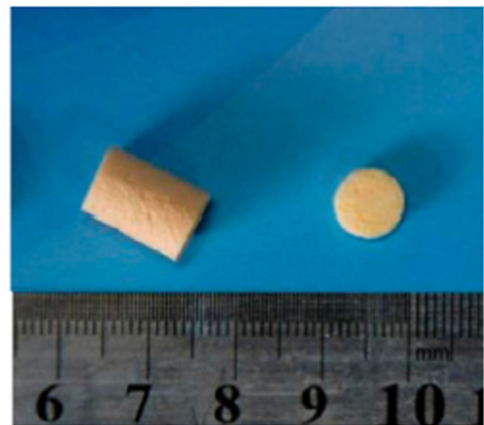


Fig. 2 The gross appearance of BP-14/gel scaffolds

polyethylene molds and aged for 24 h, followed by freezing for 8 h. The frozen samples were then stored at $-54\text{ }^{\circ}\text{C}$ for 3 h, and freeze-dried for 3 days. The freeze dried samples were then soaked in glutaraldehyde–water solution (1 wt%) for 24 h to form cross-linked scaffolds, which were further soaked in water for 48 h, with water changes every 8 h, to remove residual glutaraldehyde. Finally, porous composite scaffolds were obtained by freeze-drying for another 3 days. The optical microstructure and gross appearance of BP-14/gel scaffolds is shown in Figs. 1 and 2.

2.2 Animals and surgical procedures

All animal procedures were approved and conducted in accordance with the Approval local (Peking University Third Hospital) animal care committee and national guidelines. Twenty-four adult New Zealand white rabbits were randomly divided into three groups.

Three groups of animals were euthanized at 4, 8 and 12 weeks post-operation, respectively.

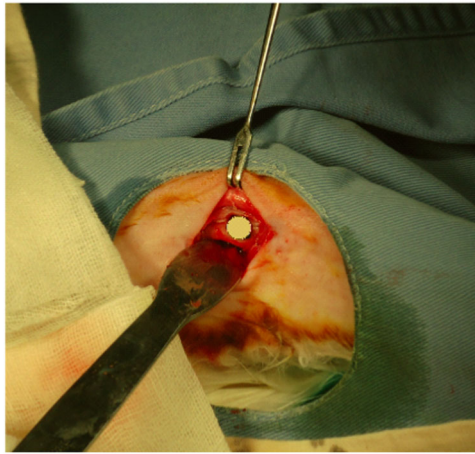


Fig. 3 Surgical site on the distal femoral of rabbit showing a circular defect filled with scaffolds

Rabbits were anaesthetized using pentobarbital sodium 20 mg/kg intramuscularly. Once the animal had reached a deep plane of anaesthesia, its lower right leg was shaved with mechanical clippers and the area cleared of fur by the application of a depilatory cream. The leg was cleaned with moist gauze and sterilized using three consecutive washes of tincture of iodine, followed by 70% ethanol. Subcutaneous injection of 1% lidocaine was administered for palliative pain prevention.

During the surgical procedure, a 2.0 cm full-thickness skin incision was made longitudinally above the lateral femoral condylar, and a needle was inserted into the joint space. Then a cavity of 5.5 mm in diameter was drilled at the center of the distal femur consecutively with different size of Kirschner wire and reaming bur, which is located about 8 mm above the knee joint. The cavity orientation was perpendicular to the longitudinal and sagittal axis of the femur. The defect site was gently cleared of blood and bone fragments with the aid of suction and tissue moist was kept by saline irrigation. After sterilizing with ethylene oxide gas, the 5.0 mm composite scaffolds were implanted into the cavities (Fig. 3) in the experimental side; in the control side, nothing was implanted. Then the fascia and skin were sutured. In post-operation, animals received topical application of 0.2% chloramphenicol antibiotic solution to the sutured skin to prevent contamination of the operated site followed by an intramuscular administration of penicillin G sodium (40wIU/d, 5 days). Rabbits were housed in well ventilated rooms and were given access to food and water.

2.3 Observation index

2.3.1 Radiological examination

To evaluate bone formation and union, standardized anterior–posterior (A–P) and lateral radiographs were taken

postoperatively on the first day and 4, 8 and 12 weeks after operation. An ultra-high definition film, 70 kV and 50 mA, with a constant X-ray-to object-to film distance of 90 cm were used.

2.3.2 Gross observation

Rabbits were sacrificed for gross observation 4, 8 and 12 weeks after surgery. Healing signs of the femur were observed.

2.3.3 Micro-computer tomography examination

At 4, 8 and 12 weeks after surgery, eight rabbits from each group were sacrificed. The specimens of each group were prepared for micro-CT scan (Siemens Inveon PET/CT). Along the long axis of the specimen, a 13.6 μm resolution scan was acquired in a consecutive micro-CT imager (500 kV, 500 μA), which included the defects of the implant site and peripheral area as a region of interest (ROI). New bone formation was visualized and analyzed by the Inveon research workplace (Siemens Medical Solutions, USA).

2.3.4 Histopathological examination

The lower limbs of each rabbit were harvested and dissected so that they were free of soft tissue. Sections containing the defect area were cut with a slow-speed saw. The specimens were fixed with a 10% neutral formalin solution for 48 to 72 h. Each specimen was demineralized for hematoxylin and eosin (H&E) staining. The specimens were decalcified with 10% EDTA, and embedded in paraffin followed with H&E staining. Sagittal sections (5 μm -thick, four sections, with two sections from the central region and another two sections from the interface between the graft and the defect) were H&E stained. Parts of these specimens were prepared for immune-histochemistry analysis, which mainly focuses on the in-growth of blood vessel, using vascular endothelial growth factor (VEGF) as the marker.

2.4 Statistical analysis

Statistical analyses were conducted using SPSS 17.0 (SPSS Inc., USA). Continuous, normally distributed variables were expressed as means \pm standard deviation, a one-way ANOVA was used to compare differences in groups, and the LSD method was used to compare differences between groups. The difference was regarded as statistically significant when $P < 0.05$. All statistical tests were two-tailed.



Fig. 4 Post-operative radiographs of each side. With the time extension, the density has further increased, and the experimental side density is higher than the control side. 1 control side; 2 experimental side; **a** 1 day, **b** 4 weeks, **c** 8 weeks, and **d** 12 weeks

3 Results

3.1 Radiological examination

Standardized A–P and lateral radiographs were taken postoperatively on the first day and 4, 8, and 12 weeks after operation. The bilateral distal femoral bone defects were visible on the first day post-operation, and the composite scaffold is radiolucent. Local density had increased 4 weeks post-operative at the defect area with ground glass tissue formation, and density of the experimental side is higher than the control side; with the time extension, the density has further increased 8 and 12 weeks post-operative in each side. The x-ray images were shown in Fig. 4.

3.2 Gross observation

All the animals tolerated the procedure well, the wound healed without obvious redness, infection and poor healing. Soft tissue was cleaned up for gross observation after specimens harvested.

3.2.1 The control side

The original bone defects were still visible 4 weeks post-operative, with the time extension, the defect area gradually healed. Cortex bone healed completely 12 weeks

postoperative. There is no new bone tissue formation in the medullary cavity when the distal femoral was slit.

3.2.2 The experimental side

The original bone defects were also visible 4 weeks post-operative and the composite scaffold exposed. When the distal femoral was slit, the composite scaffold contacted well with the surrounding tissue, without envelope and inflammatory liquid concentration. The original bone defect was mostly filled with new bone 8 weeks postoperative, the area of the composite scaffold surface shrunk, the scaffold color was similar with the surrounding tissue and could not be distinguished. The bone defect area was completely filled with new bone tissue, the scaffold integrated well into the medullary cavity, the hardness of composite scaffold area were higher than the surrounding tissue, but close to normal distal femur cancellous bone.

3.3 Micro-computer tomography

The area of new bone tissue on the experimental side is much larger than the control side analyzed by the Inveon research workplace. The new bone tissue grown from the edge to the center and gradually replaced the implant scaffold. The Micro-CT scan images of each side were shown in Figs. 5 and 6. The bone defect area was set as the

Fig. 5 Micro-CT images of the control side. There was void of new bone tissue in the bone defect area at all the time points. 1, 2, 3: 4, 8, 12 weeks, respectively; **a** axial reconstruction; **b** sagittal reconstruction

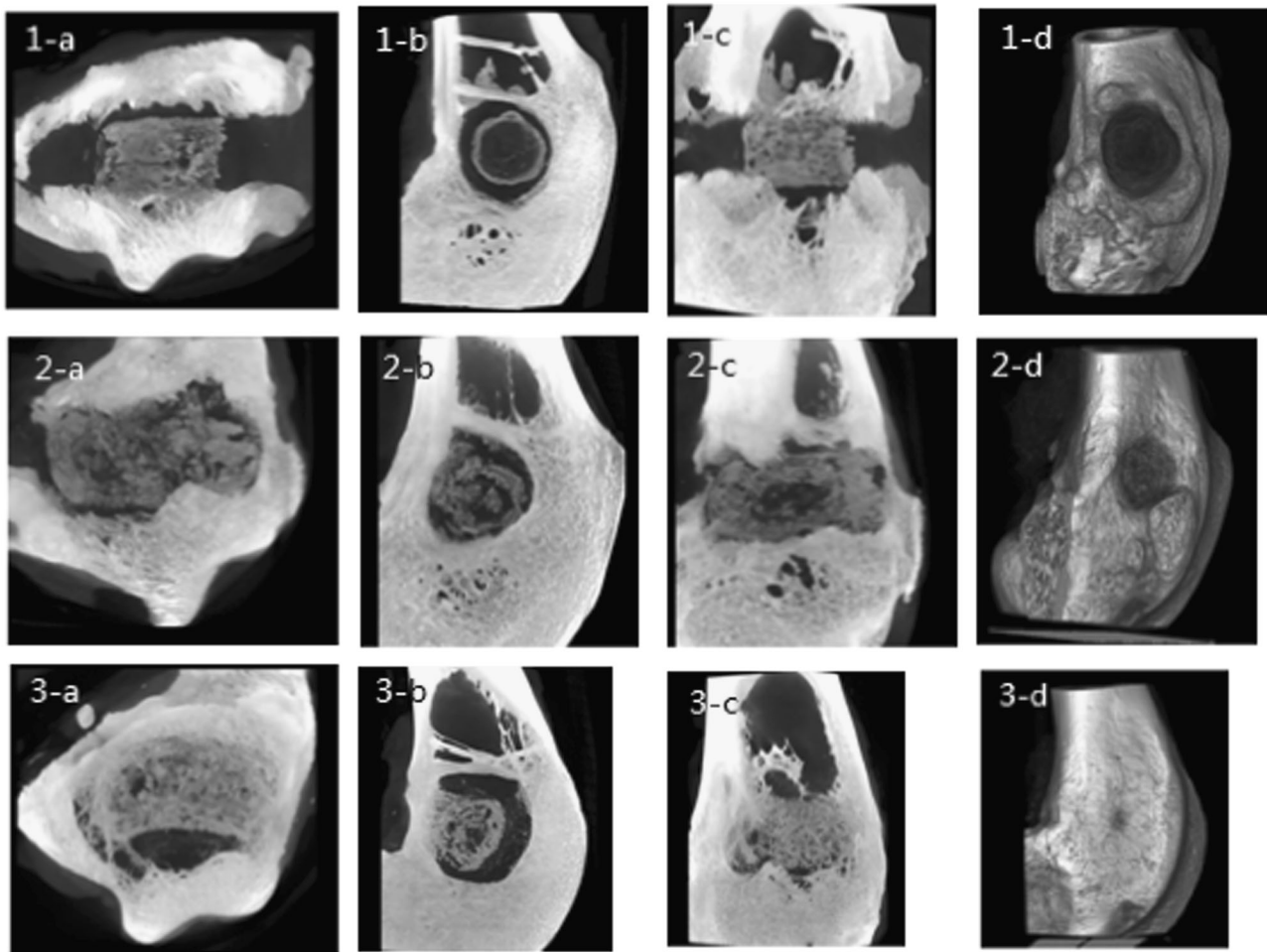
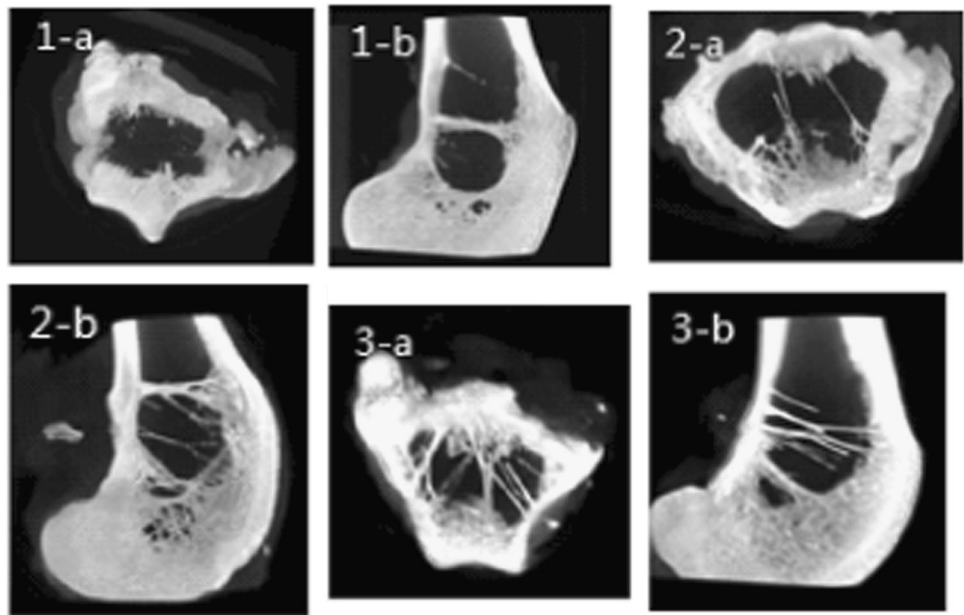
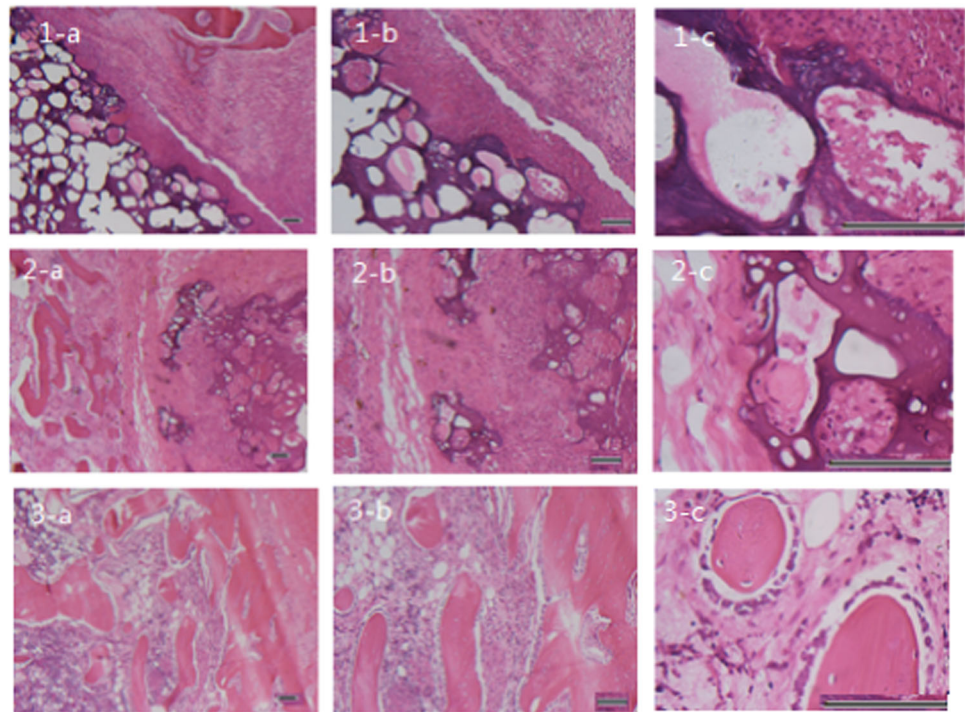


Fig. 6 Micro-CT images of the experimental side. With the time extension, the new bone tissue grown from the edge to the center and gradually replaced the implant scaffold. 1, 2, 3: 4, 8, 12 weeks,

respectively; **a** axial reconstruction; **b** sagittal reconstruction; **c** coronal reconstruction; **d** three dimensional reconstruction

Table 1 Dates measured by the Inveon research workplace analysis software

	BV/TV	BSA/BV (1/mm)	TbTh (mm)	TbN (1/mm)	TbSp (mm)
4w	0.1193 ± 0.0143	13.5991 ± 1.1468	0.1480 ± 0.0127	0.8068 ± 0.0734	1.1003 ± 0.1140
8w	0.2130 ± 0.0433	10.7045 ± 1.2738	0.1890 ± 0.0205	1.1201 ± 0.1435	0.7180 ± 0.1410
12w	0.2821 ± 0.0431	9.8358 ± 2.2293	0.2137 ± 0.0541	1.3557 ± 0.2229	0.5391 ± 0.0731
<i>P</i>	0.000	0.001	0.000	0.000	0.001

Fig. 7 Histological section of experimental side with H&E staining. 1, 2, 3: 4, 8, 12 weeks, respectively; **a** 5×; **b** 10×; **c** 40×; Scale bar 100 μm

ROI, which is 5 mm in diameter and parallel to the scaffold. Inveon research workplace analysis software was used to measure the relative bone volume (bone volume/tissue volume, BV/TV), bone surface area/bone volume (BSA/BV), trabecular thickness (TbTh), trabecular number (TbN) and the trabecular spacing (TbSp) of the experimental side 4, 8 and 12 weeks postoperative, respectively. SPSS 17.0 was used to compare the difference among groups. There were statistically significant differences among different time point all of the five indexes. With the time extension, the relative bone volume, TbTh and TbN gradually increased, while the BSA/BV and TbSp reduced. The dates were shown in Table 1.

There were statistically significant differences among different time point all of the five indexes. The relative bone volume, TbTh and TbN gradually increased, while the BSA/BV and TbSp reduced, $P < 0.05$. BV/TV bone volume/tissue volume; BSA/BV bone surface area/bone

volume; TbTh trabecular thickness; TbN trabecular number and TbSp trabecular spacing.

3.4 Histopathological examination

Histological section of experimental side with H&E staining were shown in Fig. 7. Composite scaffold maintained its original form 4 weeks postoperative with some inflammatory reaction. Macrophages, mesenchymal cells and fibroblasts were seen in the pore at the host bone-scaffold junction. A large number of cells invaded into the central part of the composite scaffold 8 weeks postoperative, and the scaffold had been partly degraded. Osteoblast and bone matrix can be seen at the high magnification field. The scaffold had been completely degraded 12 weeks postoperative, cartilage matrix calcification and woven bone formation can be seen. And there were a large number of active osteoblasts surrounded the newly formed trabecular structure.

4 Discussion

Bone defect is a common orthopedic diseases, which may lead to limb deformities, dysfunction and other complications if improperly handled. Research on the bone substitute materials in the clinical treatment of bone defects have become a hot topic. There are some disadvantages of the bone substitute materials. The fatigue strength of bio-glass is low, and the high stiffness and brittleness makes it difficult to molding and fixation. On the other hand, the degradation products of synthetic polymer materials can lead to inflammation and is not conducive to cell growth with low cell affinity. Therefore, the present osteoconductive material study focused on the composite materials, which obtain the advantage of both parts [13]. In our previous work, we have successfully combined bioactive nanoparticle and gelatin to form composite scaffolds, which are bioactive and with mechanical properties comparable to cancellous bones.

Experimental models of bone regeneration using critical defects with no spontaneous regeneration have been used to analyze different substances with osteoinductive properties, which are specifically able to induce the differentiation of osteoprogenitor cells into osteoblasts and induce bone formation [14, 15]. The purpose is to study the *in vivo* bioactivity of the scaffold we designed and verify its ability to simulate the characteristics of cancellous bone. We chose the supra-condylar area for a low demand for mechanical strength, and there is no normal cancellous bone, but red bone marrow with a large amount of osteo-progenitor cells, which can induce gather of osteoblasts and new bone formation [16]. We have found that cells could adhere, spread, and proliferate very well in the composite scaffolds. We used the Inveon research workplace to measure the relative bone volume in both the distal femoral area and the bone defect area, which is implanted by the composite scaffold. We had found that the BV/TV of normal distal femur cancellous bone area were 0.2634–0.2926, and the average BV/TV of the experimental side 12 weeks postoperative was 0.2821, there was no significant difference between the two parts. From this point of view, this new scaffold may have the ability to simulate the formation of new bone, which has a similar three dimensional structure as the normal cancellous bone.

An essential requirement for an artificial material to bond to living bone is the formation of a biologically active bone-like apatite layer on its surface in a body environment [17]. The new bone is assembled through the orderly deposition of apatite minerals within the collagen matrix [18, 19]. We have found that this composite scaffold has the suitable surface area for the induction of new bone formation, which is good for ion exchange reaction and the formation of hydroxyl apatite layer interface. Moghadam et al. [20]

indicated that only the decalcified bone matrix had the ability of bone induction and speculated that calcium salt related to BMP release. There was visible high-density material deposition around the composite scaffold 4 weeks postoperative both in the x-ray and the Micro-CT image, though there was no mature bone tissue in the corresponding H&E staining biopsy yet, we therefore speculated that the composite scaffold could induce the formation of hydroxyl carbonate apatite layer in the early stage after implantation. Micro-CT image showed that the hydroxyl carbonate apatite deposited more with the time extension, and there was visible formation of bone matrix in the H&E staining biopsy 8 weeks postoperative, which induced the formation of new bone tissue inside the scaffold further. By the time of 12 weeks, we had seen obvious trabecular bone structure formation in the H&E staining biopsy.

Osteogenesis showed a trend of “creeping substitution” process. At present, most of the bone ossification process in artificial material begun at the peripheral area and crawled to the center gradually, at the early stage, there was no new bone formation in the center of the implant [21]. The micro-CT image showed that the new bone tissue grown from the edge to the center and gradually replaced the implant scaffold with the time extension, and the 3-D reconstruction fully displayed the new bone tissue formation in the center of the scaffold. In the H&E staining biopsy, we also saw the cells invade from the edge to the center, which characterized the “creeping substitution” process. The porosity of this scaffold provided a good space for the cell metabolism and nutrient exchange, and is beneficial to the in-growth of granulation tissue and the crawl substitution of original trabecular bone.

This scaffold is a good medium for cell adhesion and with appropriate BP particle size and pore spacing, avoiding the sedimentation of big particles in the scaffolds and facilitate bone formation [22]. The gelatin is a kind of natural biodegradable protein molecules and has good biocompatibility without tissue rejection, and is an natural organic material to simulate bone tissue. Moreover, fibrin glue has no inhibitory effect on cell differentiation, proliferation and morphology [23]. And the movement of osteoblasts along the compound scaffold network resulted in bone remodeling much earlier than usual. In the H&E staining biopsy 4 weeks postoperative, there was visible cells invade the scaffold pore in the peripheral area, and cell proliferation was more and more with the time extended. All the process, there was no obvious inflammatory liquid concentration. Good biocompatibility, and the ability to promote cell adhesion, proliferation are the advantages of this new scaffold.

If there is no proper blood supply inside the scaffold, neither the bone conduction nor induction is able to complete. Rayner [24] indicated that vascularization of the

material is necessary for bone formation in the 1980s. The pore sizes of the composite scaffolds were in the range of 50 to 300 μm , which is suitable for cell adhesion and growth as well as blood vessels growth [25, 26]. The expression of vascular endothelial growth factor (VEGF) is to promote blood vessel formation condition, which provides new bone with adequate blood supply [27]. In biopsy of the experimental side, VEGF antibody detection displayed a lot of tan particles deposition in the cytoplasm, which indirectly reflect the in-growth of new blood vessels to the scaffold.

5 Conclusion

Proper bone substitute materials should have good biocompatibility and mechanical properties, and have a micro-porous structure, which is beneficial to the new born in-growth. In this experiment, cells could adhere, spread, and proliferate very well in the newly designed bioactive nanoparticle–gelatin composite scaffold. This scaffold showed good biodegradability, bioactivity and cyto-compatibility. It induced new bone formation well when it is implanted. And the mechanical properties of the scaffold and the 3-D structure of new bone tissue are comparable to cancellous bones. We speculate it may be a promising artificial bone grafts.

Acknowledgements The authors would like to thank Dr. Huijie Leng and M.M. Shang LI for their help in Micro-CT image scan and Animal experiment.

Funding This work was supported by Natural Science Foundation Of China (Project 51173193).

Compliance with ethical standards

Conflict of interest The authors declare that they have no competing interests.

References

1. Yang J, Chen HJ, Zhu XD, et al. Enhanced repair of a critical-sized segmental bone defect in rabbit femur by surface micro-structured porous titanium. *J Mater Sci Mater Med*. 2014;25(7):1747–56.
2. Janeway HH. Autoplastic transplantation of bone. *Ann Surg*. 1910;52(2):217–28.
3. Reichert JC, Saifzadeh S, Wullschlegel ME, et al. The challenge of establishing preclinical models for segmental bone defect research. *Biomaterials*. 2009;30(12):2149–63.
4. Giannoudis PV, Dinopoulos H, Tsiridis E. Bone substitutes: an update. *Inj-Int J Care Inj*. 2005;36 Suppl 3(11):20–7.
5. Calori GM, Mazza E, Colombo M, et al. The use of bone-graft substitutes in large bone defects: any specific needs? *Inj-Int J Care Inj*. 2011;42 Suppl 2(3):S56–63.
6. Valliant EM, Jones JR. Softening bioactive glass for bone regeneration: sol–gel hybrid materials. *Soft Matter*. 2011;7(11):5083–95.
7. Azami M, Moztaarazadeh F, Tahiri M. Preparation, characterization and mechanical properties of controlled porous gelatin/hydroxyapatite nanocomposite through Layer solvent casting combined with freeze-drying and lamination techniques. *Porous Mater*. 2010;17:313–20.
8. Kim HW, Kim HE, Salih V. Stimulation of osteoblast responses to biomimetic nanocomposites of gelatin–hydroxyapatite for tissue engineering scaffolds. *Biomaterials*. 2005;26(25):5221–30.
9. Gentile P, Mattioli-Belmonte M, Chiono V, et al. Bioactive glass/polymer composite scaffolds mimicking bone tissue. *J Biomed Mater Res Part A*. 2012;100a(10):2654–67.
10. Ma PX. Biomimetic materials for tissue engineering. *Adv Drug Deliv Rev*. 2008;60(2):184–98.
11. Chen W, Yue X, Li A, et al. Bioactive nanoparticle through postmodification of colloidal silica. *ACS Appl Mater Interfaces*. 2014;6(7):4935–4939.
12. Wang C, Shen H, Tian Y, et al. Bioactive nanoparticle-gelatin composite scaffold with mechanical performance comparable to cancellous bones. *ACS Appl Mater Interfaces*. 2014;6(15):13061–8.
13. Sachlos E, Czernuszka JT. Making tissue engineering scaffolds work. Review: the application of solid freeform fabrication technology to the production of tissue engineering scaffolds. *Eur Cells Mater*. 2003;5:29–39.
14. Hollinger JO, Kleinschmidt JC. The critical size defect as an experimental model to test bone repair materials *J Craniofac Surg*. 1990;1(1):60–8.
15. Mish CE, Dietsch F. Bone grafting materials in implant dentistry. *Implant Dent*. 1993;2(3):158–67.
16. Rosselli JEGC, Martins DMFS, Martins JL, et al. The effect of simvastatin on the regeneration of surgical cavities in the femurs of rabbits. *Acta Cir Bras*. 2014;29(2):87–92.
17. Kokubo T, Kushitani H, Sakka S, et al. Solutions able to reproduce in vivo surface-structure changes in bioactive glass-ceramic A-W3. *J Biomed Mater Res*. 1990;24(6):721–34.
18. Cui FZ, Li Y, Ge J. Self-assembly of mineralized collagen composites. *Mater Sci Eng R Rep*. 2007;57(1):1–27.
19. Müller R. Hierarchical microimaging of bone structure and function. *Nat Rev Rheumatol* 2009;5(7):373–81.
20. Moghadam HG, Sándor GKB, Holmes HHI, et al. Histomorphometric evaluation of bone regeneration using allogeneic and alloplastic bone substitutes. *J Oral Maxillofac Surg*. 2004;62(2):202–13.
21. Niu X, Fan Y, Liu X, et al. Repair of bone defect in femoral condyle using microencapsulated Chitosan, Nanohydroxyapatite/Collagen and Poly(L-Lactide)-based microsphere-scaffold delivery system. *Artif Organs*. 2011;35(7):E119–28.
22. Wozney J, Rosen V. Bone morphogenetic protein and bone morphogenetic protein gene family in bone formation and repair. *Clin Orthop Relat Res*. 1998;346(346):26–37.
23. Chen Y, Bai B, Zhang S, et al. Study of a novel three-dimensional scaffold to repair bone defect in rabbit. *J Biomed Mater Res Part A*. 2014;102(5):1294–1304.
24. Rayner CR. The healing of autologous bone grafts after varying degrees of surgical trauma. A microscopic and histochemical study in the rabbit. *J Bone Jt Surg Br Vol*. 1980;62(3):403–10.
25. Tavakol S, Azami M, Khoshzaban A, et al. Effect of laminated hydroxyapatite/gelatin nanocomposite scaffold structure on

- osteogenesis using unrestricted somatic stem cells in rat. *Cell Biol Int.* 2013;37(11):1181–9.
26. Janicki P, Schmidmaier G. What should be the characteristics of the ideal bone graft substitute? Combining scaffolds with growth factors and/or stem cells. *Inj-Int J Care Inj.* 2011;42 Suppl 2(3): S77–S81.
27. Gao W, Xing Q, Ma S, et al. Adipose-derived stem cells accelerate neovascularization in ischaemic diabetic skin flap via expression of hypoxia-inducible factor-1 α . *J Cell Mol Med.* 2011;15(12):2575–85.